

A Synthetic Route for Crystals of Woven Structures, Uniform Nanocrystals, and Thin Films of Imine Covalent Organic Frameworks

Yingbo Zhao,^{†,#} Lei Guo,^{†,#} Felipe Gándara,^{‡,§} Yanhang Ma,[§] Zheng Liu,[⊥] Chenhui Zhu,[∇] Hao Lyu,[†] Christopher A. Trickett,[†] Eugene A. Kapustin,[†] Osamu Terasaki,[§] and Omar M. Yaghi^{*,†,⊙}

[†]Department of Chemistry, University of California-Berkeley, Materials Sciences Division, Lawrence Berkeley National Laboratory, Kavli Energy NanoSciences Institute, Berkeley, California 94720, United States

[‡]Department of New Architectures in Materials Chemistry, The Materials Science Factory, Instituto de Ciencia de Materiales de Madrid – CSIC, Madrid 28049, Spain

[⊥]Inorganic Functional Materials Research Institute, AIST, Nagoya 463-8560, Japan

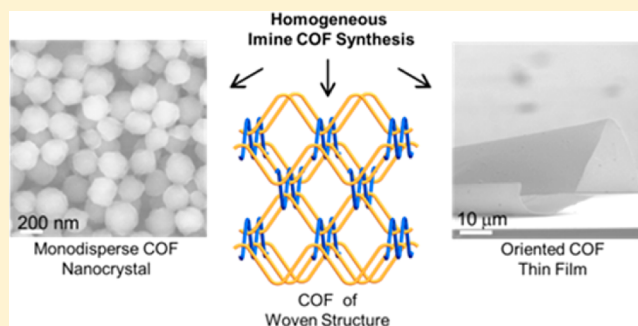
[∇]Advanced Light Source, Lawrence Berkeley National Lab, Berkeley, California 94720, United States

[§]School of Physical Science and Technology, ShanghaiTech University, Shanghai 201210, China

[⊙]King Abdulaziz City for Science and Technology, Riyadh 11442, Saudi Arabia

Supporting Information

ABSTRACT: Developing synthetic methodology to crystallize extended covalent structures has been an important pursuit of reticular chemistry. Here, we report a homogeneous synthetic route for imine covalent organic frameworks (COFs) where crystallites emerge from clear solutions without forming amorphous polyimine precipitates. The key feature of this route is the utilization of *tert*-butyloxycarbonyl group protected amine building blocks, which are deprotected *in situ* and gradually nucleate the crystalline framework. We demonstrate the utility of this approach by crystallizing a woven covalent organic framework (COF-112), in which covalent organic threads are interlaced to form a three-dimensional woven framework. The homogeneous imine COF synthesis also enabled the control of nucleation and crystal growth leading to uniform nanocrystals, through microwave-assisted reactions, and facile preparation of oriented thin films.



INTRODUCTION

The development of reticular chemistry has hinged upon our ability to crystallize the products of linking molecular building blocks by strong bonds into extended porous structures. In the original synthesis of metal–organic frameworks (MOFs), the key discovery for obtaining them as crystals was the control of deprotonation of the acid organic linkers and in turn the rate of reaction with metal ions.¹ The fact that the starting points of these reactions are homogeneous solution mixtures allowed control of nucleation and crystal growth using various synthetic methods,² and this has led to the vast expansion of MOF synthesis.³ In contrast, the synthesis of covalent organic frameworks (COFs) generally starts with heterogeneous amorphous solids resulting from the linking of organic building blocks.⁴ These solids are annealed by heating to potentially obtain microcrystalline materials; an aspect that leads to lack of control in making COFs and severely limits the possibilities for controlling their nucleation and crystal growth. Here, we report a synthetic route for making COFs that starts with a homogeneous mixture of the organic building units, demonstrates its utility for imine-based COFs, and shows how it has led to (a) the synthesis of COF-112 as crystals composed of

polyimine threads brought together by cobalt ions and interlaced to yield a woven structure, (b) size and shape controlled, uniform nanocrystals of several other COFs (LZU-1,⁵ TFPB-PDA COF,⁶ and Por-COF,⁷), and (c) facile preparation of oriented thin films of LZU-1. We believe this homogeneous synthetic route will vastly expand our ability to access crystalline COFs.

In conventional imine COF synthesis, amine and aldehyde building blocks usually form amorphous polyimine precipitates upon their reaction in solvent mixtures containing aqueous acetic acid catalyst. The resulting heterogeneous mixture gradually turns into aggregates of microscopic COF crystallites after being heated in sealed Pyrex tubes for days.⁸ Typically, the imine COFs thus obtained have morphology resembling the initial polyimine precipitates, as the COF nucleation and growth are intrinsically heterogeneous and insensitive to the addition of modulators. In this process, crystallization relies on the reversible imine condensation reaction to correct defects in the polyimine precipitate. This process would not be successful

Received: July 17, 2017

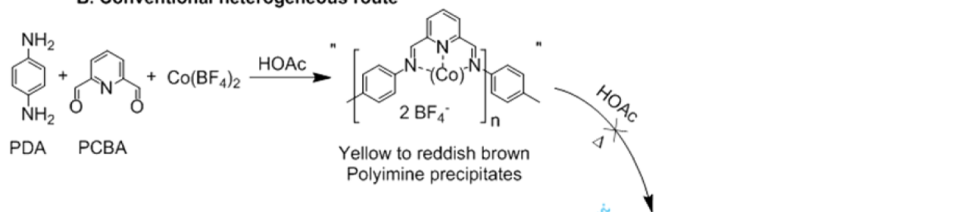
Published: August 28, 2017

Scheme 1. Conventional Heterogeneous, Homogeneous (One-Pot), and Metal-Complex Route for Crystalline Woven COF-112

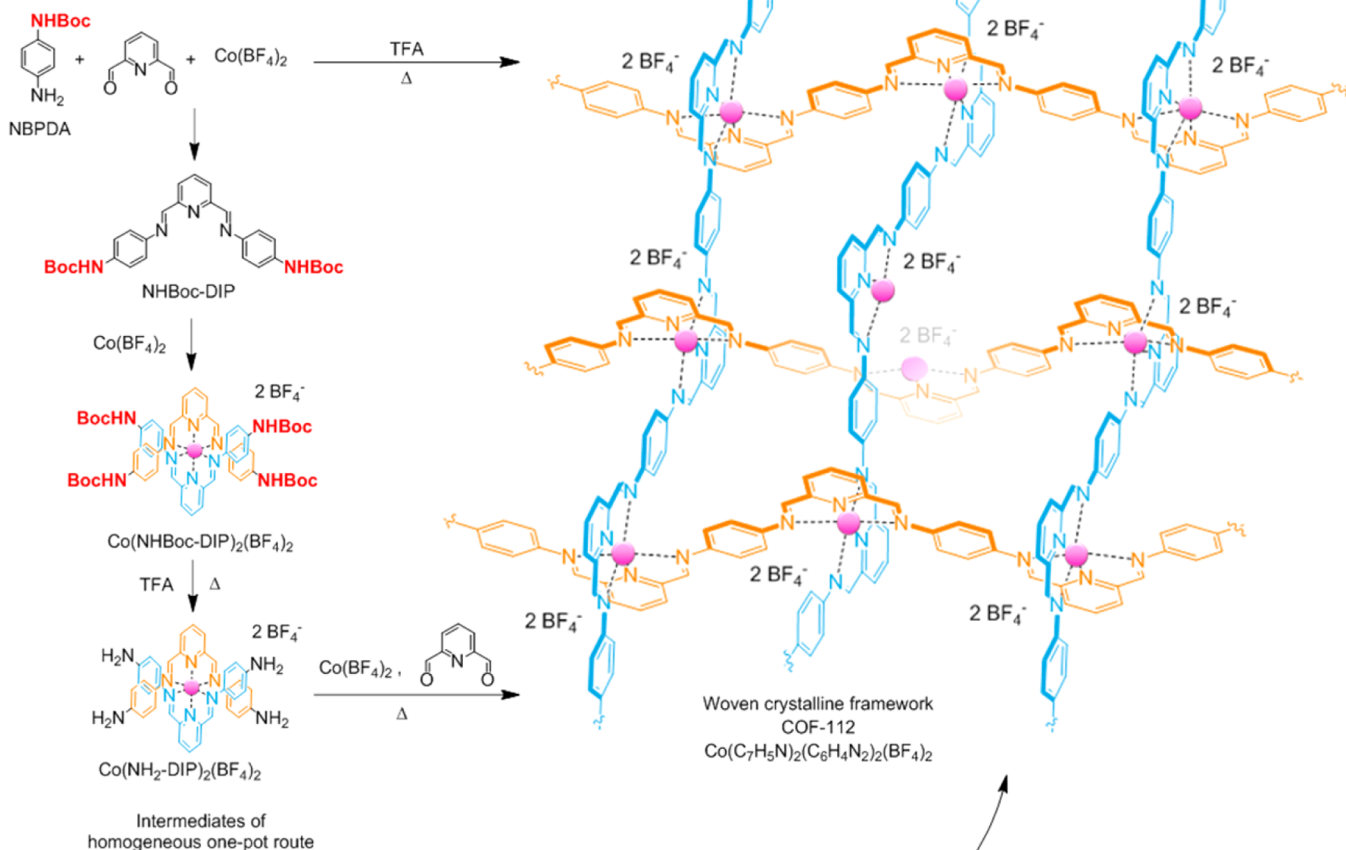
A. Cobalt bis(diiminopyridine) complex



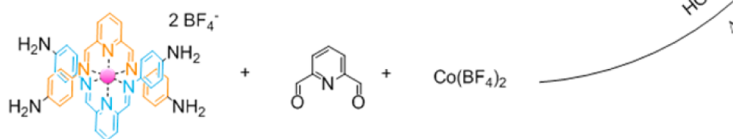
B. Conventional heterogeneous route



C. Homogeneous one-pot route



D. Metal-complex route



if substantial structural difference is present between the desired COF and the polyimine precipitate. Such limitations have in turn restricted access to crystalline COFs and the scope of their synthesis. In this study, we address this challenge by the utilization of the *tert*-butyloxycarbonyl (Boc) group protected amine as the starting reagent to synthesize COFs homogeneously rather heterogeneously. The amine can be gradually deprotected *in situ* with trifluoroacetic acid to slow down the imine condensation reaction and facilitate COF crystallization. This synthetic route thus enables imine-based COFs to be synthesized homogeneously without the usual complications of having amorphous insoluble intermediates. We demonstrate the power of this synthetic approach by synthesizing imine

COFs as crystals of woven structures, uniform nanocrystals, and thin films.

EXPERIMENTAL SECTION

Chemicals. Co(BF₄)₂·6H₂O, *p*-phenylenediamine (PDA), poly(vinylpyrrolidone) (PVP, *M_w* = 10,000 and 360,000), ethanol (anhydrous, ≥99.5%), and triethylamine (TEA) were obtained from Sigma-Aldrich. 1,3,5-Triformylbenzene (TFB, ≥98%), 4-(*tert*-butoxycarbonylamino)-aniline (NBPDA), and acetone were obtained from Acros Organics. 2,6-Pyridinedicarboxaldehyde (PCBA, ≥98%) was obtained from TCI. Toluene (≥99.8%), acetonitrile (≥99.8%), glacial acetic acid, and trifluoroacetic acid (TFA, ≥99.7%) were obtained from EMD Millipore Chemicals. All starting materials, reagents, and solvents were used without further purification.

Analytical Techniques. Gas adsorption experiments were carried out on a Quantachrome AUTOSORB-1 automatic volumetric instrument. Ultrahigh-purity-grade N₂ and He gases were used in all adsorption measurements. The N₂ (77 K) isotherms were measured using a liquid nitrogen bath (77 K). The backbone density of the COF-112 was measured by pycnometry on a Quantachrome-UPYC 1200e V5.04 instrument using He gas. Powder X-ray diffraction (PXRD) patterns were recorded using a Rigaku Miniflex 600 (Bragg–Brentano geometry, Cu K_α radiation $\lambda = 1.54 \text{ \AA}$) diffractometer. Solution ¹H NMR spectra were acquired on a Bruker AVB-400 and AV-600 NMR spectrometer. Elemental microanalyses (EA) were performed in the Microanalytical Laboratory of the College of Chemistry at UC Berkeley, using a PerkinElmer 2400 Series II CHNS elemental analyzer. The amount of Co, Fe, and B in COF-112 was analyzed by ICP–AES spectroscopy with an Optima 7000 DV (PerkinElmer) instrument. Attenuated total reflectance (ATR) FTIR spectra of neat samples were performed on a Bruker ALPHA Platinum ATR-FTIR spectrometer equipped with a single reflection diamond ATR module. Scanning electron microscope (SEM) images were recorded on a Zeiss Gemini Ultra-55 analytical SEM with accelerating voltage of 5 kV. Transmission electron microscopy (TEM) was performed on a cold field emission JEM-2100F instrument equipped with a DELTA C_s corrector. Optical refractive index was measured using ellipsometer (Gaertner Scientific Corporation). Single crystal X-ray diffraction data were collected using synchrotron radiation on beamline 11.3.1 at the Advanced Light Source (ALS) at Lawrence Berkeley National Lab (LBNL), equipped with a Bruker Photon 100 CMOS area detector using synchrotron radiation (16 keV). Samples were mounted on MiTeGen kapton loops and placed in a 100 K nitrogen cold stream. Grazing-incidence wide-angle X-ray scattering (GIWAXS) patterns were acquired with a Pilatus 2 M (Dectris) instrument on beamline 7.3.3 at the ALS ($\lambda = 1.24 \text{ \AA}$). The incidence angle was held at 0.120° to optimize signal collection. Silver behenate was used for calibration. The Nika package for IGOR Pro was used to reduce the acquired 1D raw data to a 2D format.

Homogeneous One-Pot Synthesis of COF-112. A Pyrex tube measuring 10 × 8 mm (o.d. × i.d.) was loaded with PCBA (5.4 mg, 0.04 mmol), NBPDA (8.3 mg, 0.04 mmol), Co(BF₄)₂·6H₂O (6.8 mg, 0.02 mmol), 0.3 mL of acetonitrile, 0.4 mL of toluene, and 0.05 mL of aqueous TFA solution (TFA:water, 1:4) (Scheme 1). The tube was flash frozen at 77 K (liquid N₂ bath), evacuated to an internal pressure of 50 mTorr, and flame-sealed. Upon sealing, the length of the tube was reduced to 18–20 cm. The reaction was heated at 85 °C for 48 h, yielding brown solids at the bottom of the tube. The product was isolated by centrifugation and washed with acetone and dried at 120 °C at 50 mTorr for 12 h. This material is insoluble in water and common organic solvents such as hexanes, methanol, acetone, tetrahydrofuran, *N,N*-dimethylformamide, and dimethyl sulfoxide, indicating the formation of an extended covalent structure.

Metal-Complex Synthesis of COF-112. A Pyrex tube measuring 10 × 8 mm (o.d. × i.d.) was loaded with Co(NH₂-DIP)₂(BF₄)₂ (8.6 mg, 0.01 mmol), PCBA (2.7 mg, 0.02 mmol), Co(BF₄)₂·6H₂O (3.4 mg, 0.01 mmol), 0.4 mL of acetonitrile, 0.6 mL of toluene, and 0.1 mL of 6 M aqueous acetic acid solution. The tube was flash frozen at 77 K (liquid N₂ bath), evacuated to an internal pressure of 50 mTorr, and flame-sealed. Upon sealing, the length of the tube was reduced to 18–20 cm. The reaction was heated at 120 °C for 72 h, yielding brown solids at the bottom of the tube. The solids were isolated by centrifugation, washed with acetone, and then dried at 120 °C at 50 mTorr for 12 h. EA of COF-112: Calculated for C₂₆H₁₈N₆Co₁B₂F₈·2H₂O = Co(C₇H₅N)₂ (C₆H₄N₂)₂(BF₄)₂: C, 45.72; H, 3.25; N, 12.30%. Found: C, 45.57; H, 3.81; N, 12.05%. FTIR: 1622 (m), 1587 (m), 1496 (m), 1284 (w), 1166 (w), 1053 (s), 957 (m), 833 (m).

Synthesis of LZU-1 Nanocrystals. TFB (5 mg, 0.03 mmol), NBPDA (10 mg, 0.05 mmol), and PVP (*M_w* = 360,000, 20 mg) were dissolved in 2 mL of ethanol and 0.24 mL of TFA. The solution was transferred to a 10 mL glass microwave vessel and heated to 120 °C for 30 min. The reddish dispersion obtained was diluted with ethanol to 8 mL and centrifuged at 8000 rpm for 5 min. The red solid collected was dispersed into 8 mL ethanol and 0.5 mL TEA to give a

yellow suspension. The color change indicated the protonated imine in the nanocrystals were deprotonated by the amine base. The solution was centrifuged again at 8000 rpm to collect the nanocrystals, and the supernatant was decanted. The yellow solid collected can be then redispersed in polar solvents such as ethanol, methanol, and *N,N*-dimethylformamide. For larger nanocrystals with size of 500 nm, 10 mg of PVP (*M_w* = 360,000) instead of 20 mg of PVP was used in the same synthetic procedure. For nanocrystals with sizes of 112 nm, the growth solution was prepared to have TFB (5 mg, 0.03 mmol), NBPDA (10 mg, 0.05 mmol), and 40 mg PVP (*M_w* = 10,000) dissolved in 1 mL of ethanol and 0.12 mL of TFA. For hexagonal shaped nanocrystals, a toluene/ethanol = 1:9 mixture was used instead of pure ethanol as the solvent. FTIR: 1617 (s), 1493 (s), 1248 (w), 1145 (s), 968 (m), 835 (s) (Supporting Information, Section S9).

Synthesis of LZU-1 Thin Films. The growth of LZU-1 thin film was realized by suspending the substrate into a heated growth solution at a constant temperature of 100 °C with reaction time varied between 1.5 and 6 h depending on the desired thicknesses. The growth solution was prepared by dissolving TFB (5 mg, 0.03 mmol) and NBPDA (10 mg, 0.05 mmol) in a solvent mixture of 2.25 mL of toluene, 0.75 mL of dioxane, and 0.6 mL of TFA. The as-prepared thin films were washed with the dioxane/TEA mixture and dried under a stream of nitrogen.

RESULTS AND DISCUSSION

We showed in a previous report on the first woven COF (COF-505) that an aldehyde functionalized derivative of the copper bis-phenanthroline complex can be used as a starting point, where the positions of the aldehyde groups approximate a tetrahedral geometry. This complex was linked with benzidine to form a framework of diamond topology having one-dimensional (1D) polyimine threads woven around the coordinated copper(I) ions.⁹ In this copper *bis*-phenanthroline complex, the dihedral angle between the two phenanthroline rings is 57°, which gives a distorted tetrahedral coordination geometry of copper(I) ion and directs the polyimine chains to be helical and mutually woven in the COF-505 structure. We sought to use a less distorted tetrahedral building unit having symmetrical arrangement of the organic threads to give an ideal woven structure based on the diamond topology. Accordingly, we recognized that this might be realized by employing cobalt bis(diiminopyridine) complexes [Co (DIP)₂] as the tetrahedral building unit having dihedral angles (between the two pyridine rings) of 80°, close to the ideal angle of 90° (Scheme 1A).¹⁰ Since the Schiff base diiminopyridine (DIP) ligand can be synthesized through imine condensation, conventional one-pot COF synthesis was initially set up with PDA, PCBA, and Co(BF₄)₂·6H₂O as starting materials (Scheme 1B). However, this yielded no crystalline product despite testing a wide range of synthetic conditions. Throughout this process, we observed that yellow precipitates often formed initially that quickly turned reddish brown. An observation indicating imine condensation has proceeded to give polyimine precipitate before all the DIP sites are coordinated by cobalt. Since the nonmetalated polyimine threads can be crystallized and they were found to pack into structures dramatically different from that of the targeted woven framework (Supporting Information, Section S3), we speculated and observed that defect correction with conventional solvent annealing is insufficient to afford crystalline products (Scheme 1B). Consequently, to obtain the target crystalline woven COF, the formation of polyimine precipitates needed to be avoided to allow the metal DIP complexes to direct the propagation and entanglement of the polyimine chains. Thus, we employed NBPDA as the starting material where one of the two amine groups in PDA is protected with a Boc group, which can form the DIP ligand and

corresponding cobalt complexes rapidly at room temperature (Scheme 1C), yet avoid the precipitation of the polyimine observed in the heterogeneous route (Scheme 1B). We note that this methodology is fundamentally different from the previously reported boronic ester COF synthesis with protected catechol, where the protecting groups are introduced to incorporate otherwise insoluble and unstable building blocks.¹¹ This boronic ester reaction to make COFs is usually homogeneous, unlike the imine COF reactions discussed in this report.

The one-pot homogeneous synthesis of COF-112 was thus carried out with NBPDA, PCBA, and $\text{Co}(\text{BF}_4)_2$ as starting materials in a solvent mixture of acetonitrile and toluene with trifluoroacetic acid as the catalyst for imine condensation and the deprotection reagent for the Boc group (Scheme 1C). This clear solution was heated in a sealed Pyrex tube at 85 °C for 48 h, to yield reddish brown microcrystals. In this synthetic route, NBPDA and PCBA first undergo imine condensation to form the Boc-protected diiminopyridine ligand (NHBoc-DIP, Scheme 1C). This rapidly binds cobalt ions to form the $\text{Co}(\text{NHBoc-DIP})_2(\text{BF}_4)_2$ complex giving the red color to the homogeneous solution. While being heated, crystalline solids emerged from this red solution as the *in situ* deprotected amine groups reacted with the remaining PCBA to form the interlacing 1D polyimine chains and the COF-112 structure (Scheme 1). In this homogeneous synthetic route to COF-112, the building up of the molecular threads is being directed by the metal complex leading to successful crystallization. This is in contrast with the unsuccessful heterogeneous route, where the polyimine chains formed prior to metal complexation (Scheme 1B). To further compare the homogeneous and heterogeneous synthesis routes, the deprotected amine intermediate $[\text{Co}(\text{NH}_2\text{-DIP})_2(\text{BF}_4)_2]$ of the homogeneous route was used to react with PCBA and the cobalt salt (Scheme 1D) in an imine COF synthesis similar to that leading to COF-505. This metal-complex route also gave crystalline COF-112, indicating the initial cobalt complex formation in the homogeneous one-pot route is the key to obtaining crystallinity.

We found that reacting the polyimine precipitate, resulting from PCBA and PDA (in the absence of cobalt), with $\text{Co}(\text{BF}_4)_2$ in the presence of acid catalyst gave amorphous product (Supporting Information, Section S3). Thus, we concluded that the utilization of the protected amine homogenizes imine COF synthesis and enables the metal–ligand coordination reaction to occur prior to polyimine chain formation, and this leads to the successful crystallization of woven COF-112. It is worth noting that the $\text{Co}(\text{NH}_2\text{-DIP})_2(\text{BF}_4)_2$ used in the metal-complex route should be perceived as an isolated reaction intermediate instead of an amine building block, as it was observed to dynamically disassemble under the *de novo* COF synthesis (Supporting Information, Section S4). The crystallites produced in this metal-complex route were also small and highly aggregated (Figure S4), while the homogeneous one-pot route with NBPDA gave larger, discrete crystals that can be studied by 3D electron diffraction tomography (3D-EDT) for COF structural determination.¹²

The completeness of the imine condensation to make COF-112 was assessed by IR spectroscopy where no vibrational modes were observed for any unreacted amine, aldehyde, and Boc protecting group (Supporting Information, Section S5). The presence of the DIP was supported by comparing the IR

spectrum with $\text{Co}(\text{NH}_2\text{-DIP})_2(\text{BF}_4)_2$. Solid-state UV–vis spectroscopy combined with inductively coupled plasma atomic emission spectroscopy (ICP-AES) and elemental analysis further confirmed the composition of COF-112 (Supporting Information, Section S5). The crystal structure of COF-112 was solved by a combination of X-ray and electron crystallographic studies (Figure 1). One three-dimensional (3D) electron

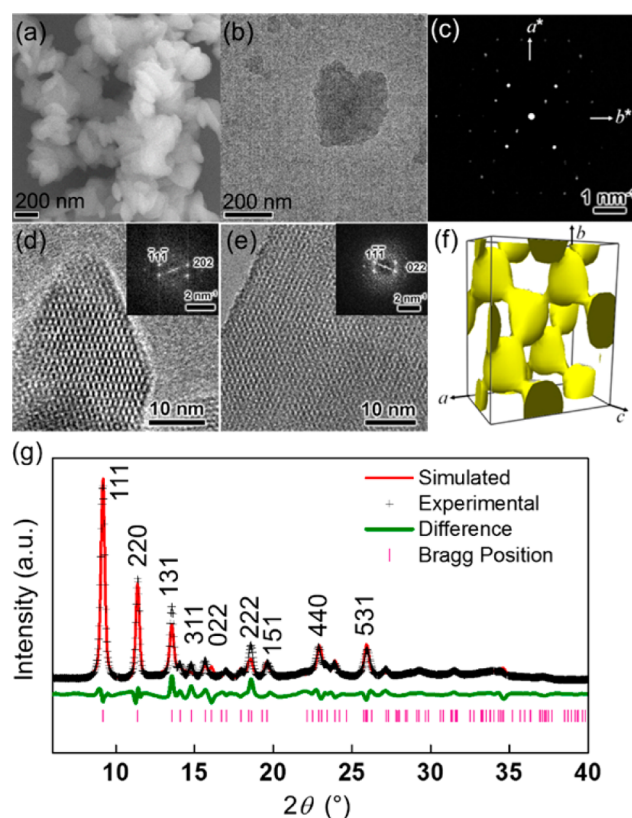


Figure 1. Structural determination of COF-112. The COF-112 crystals were 200 nm in size as observed by SEM (a). 3D-EDT study (b and c) gave the unit cell parameters a and b , from which the unit cell can be determined by Pawley refinement of the powder X-ray diffraction pattern. HRTEM images (d and e) were combined to give the cobalt positions by Fourier analysis (f). The COF-112 structural model was thus built and optimized by Rietveld refinement with R_p and R_{wp} values of 1.66% and 2.48%, respectively (g).

diffraction tomography data set was collected from a submicron crystal by using a goniometer tilt of 3° and an electron-beam tilt of 0.3° (Figure 1a–c). From the reconstruction of the reciprocal lattice, two of the unit cell parameters were uniquely determined, while the third one remained uncertain due to insufficient reflections and possible twinning. Subsequently, the PXRD pattern was indexed confirming an orthorhombic lattice and providing the third cell parameter. Pawley refinement was then conducted with the data from the PXRD pattern, resulting in unit cell parameters $a = 19.74$ Å, $b = 25.13$ Å, and $c = 12.26$ Å. The first four strong reflections in the PXRD pattern can be indexed as (111), (220), (131) and (040). The observed reflection conditions from electron diffraction and PXRD patterns were summarized as $hkl: h + k, h + l, k + l = 2n; 0kl: k, l = 2n$ and $k + l = 4n$. This indicated an F-center Bravais lattice and the most likely space group of $Fdd2$. Two high-resolution TEM (HRTEM) images of COF-112 were taken along the $[101]$ and $[0\bar{1}1]$ incidences (Figure 1d and e). The Fourier

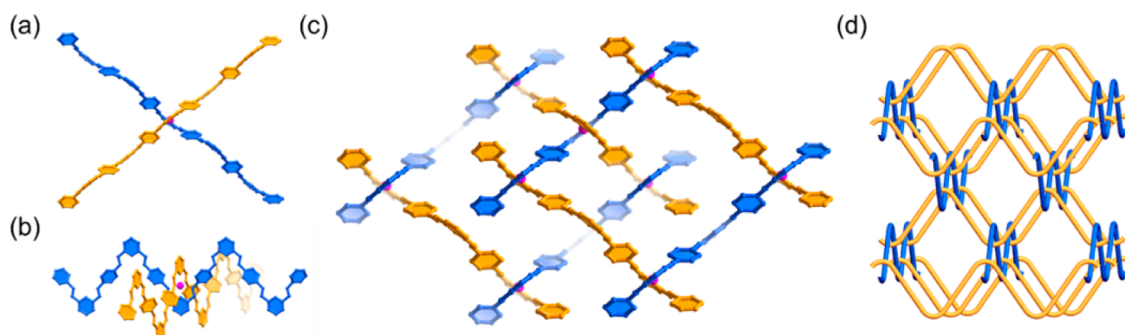


Figure 2. Structure of COF-112. (a) COF-112 is composed of two sets of interlacing polyimine threads (marked blue and orange for their different propagating directions) crossing at 77.3° angle (a). The threads are woven with cobalt(II) ions as point of registry at a regular interval of 1.6 nm (b), which form a 3D framework (c) that represents a simple 3D woven network (d). Additional parallel threads are omitted for clarity in (c).

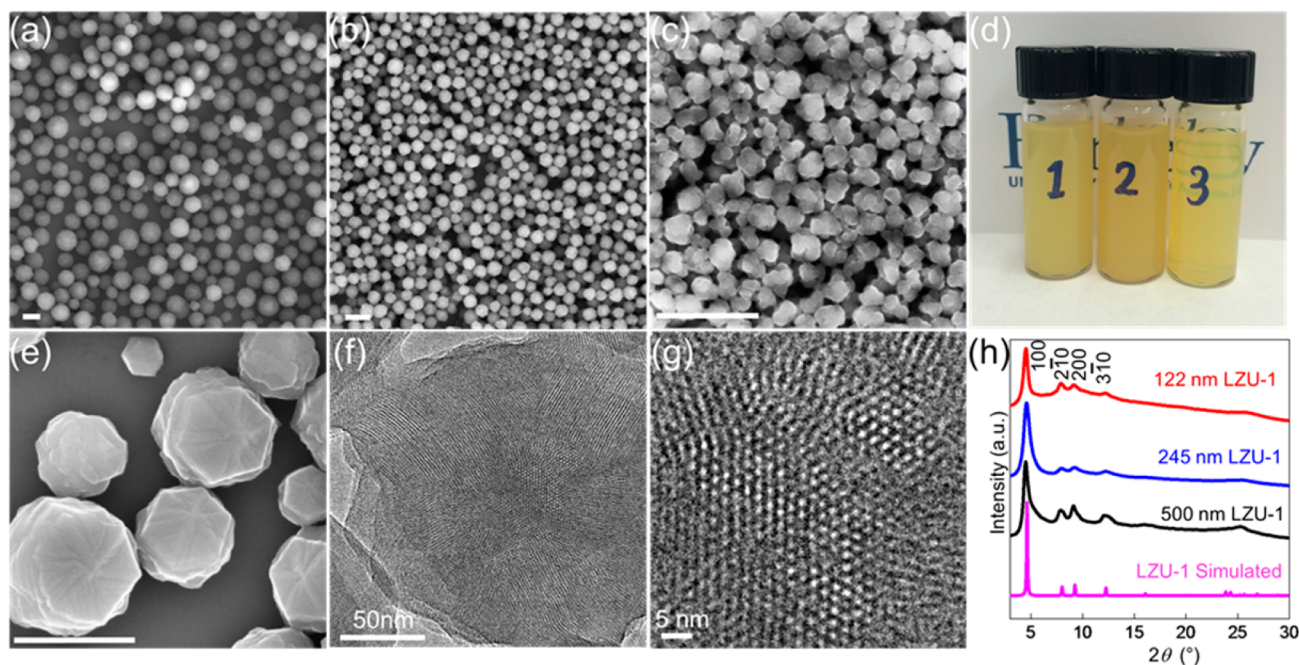


Figure 3. Size of uniform LZU-1 nanocrystals can be tuned from 500 ± 52 nm (a), 245 ± 25 nm (b), to 112 ± 11 nm (c) by tuning the concentration of PVP. These nanocrystals are highly dispersible and colloidally stable (d). By addition of toluene, hexagonal LZU-1 nanocrystals can be obtained (e). HRTEM reveals LZU-1 nanocrystals are consist of several crystalline domains, as both 1D channels (2.2 nm wide) and hexagonal pores (2.2 nm diameter) can be observed in one particle (f), which is shown in higher magnification (g). Powder X-ray diffraction shows high crystallinity of all these nanocrystals (h). Scale bar is 500 nm for (a–c) and (e).

analysis of two HRTEM images after imposing the space group symmetry indicated the positions of the cobalt centered complexes, which was consistent with that given by the electron density map reconstructed by applying the charge flipping method with the reflection intensities extracted from the PXRD pattern (Figure 1f). Moreover, with the unit cell and space group determined, the position of cobalt atoms can also be confirmed from the measured sample density of 1.4 g/cm^3 . This indicated one unit cell has only eight cobalt atoms, and their coordinates can be determined from the Wyckoff positions (Supporting Information, Section S6). The structural model of COF-112 was thus built and geometrically optimized using Materials Studio software by putting the diiminopyridine ligand around these cobalt atoms under the constraint of *Fdd2* symmetry (Supporting Information, Section S6). This model was further optimized by Rietveld refinement against the experimental PXRD pattern to give the COF-112 structure.

The structure of the COF-112 consists of two sets of 1D zigzag polyimine chains, which propagate linearly along $[110]$ and $[\bar{1}\bar{1}0]$ direction of the crystal and weave at the coordinated cobalt ions as the point of registry at regular interval of 1.6 nm (Figure 2). This structure is an ideal example of molecular weaving, which represents one of the simplest 3D woven structures, as it involves only two sets of threads that are straight and parallel and one point of registry. COF-112 is a non-interpenetrated COF with *dia* topology, with the $\text{Co}(\text{DIP})_2^{2+}$ complex considered as the tetrahedral building unit. The two sets of polyimine chains cross at an angle of 77.3° , close to the 80° dihedral angle between the two pyridine rings in the $\text{Co}(\text{NH}_2\text{-DIP})_2(\text{BF}_4)_2$ complex (Supporting Information, Section S7), thus supporting our initial design principle that the coordination geometry of the metal template would direct the propagation of the molecular threads. Additionally, an isostructural COF-112-Fe was made with iron(II) instead of cobalt(II) as the point of registry. Preliminary attempts to

demetallate COF-112 and its iron analogue were unsuccessful and require more elaborate efforts due to the kinetic inertness of the $M(\text{DIP})_2^{2+}$ ($M = \text{Co}, \text{Fe}$) complexes.^{10c} However, it should be mentioned that since tracing the threads throughout the structure is not interrupted by metal ions, their persistence in the structure is fundamentally independent of the threads. With these compounds, we sought to demonstrate the versatility of the bis-diiminopyridine metal complex templates in woven COF synthesis (Supporting Information, Section S8). Fundamentally, the COF-112 framework is an example of constructing a highly complex structure from simple building blocks, where metal coordination and imine condensation reactions take place coherently in a one-pot reaction enabled by a homogenized imine COF synthetic route.

In the homogenized imine COF synthesis, nuclei form from clear solution and grow directly into crystalline frameworks, thus opening up opportunities for COF nucleation and growth control. Specifically, a “burst of nucleation” induced by rapid heating combined with modulator regulated growth would give uniform nanocrystals, while under mild heating, the nucleation barrier would facilitate the growth of COFs on substrates. We first demonstrate this nucleation and growth control on a prototype imine COF, LZU-1, before generalization to other ones.

The slow *in situ* deprotection of amines is expected to facilitate crystallization and enable unprecedented growth of crystalline imine COFs that are only known in keto-enamine COF synthesis.¹³

Uniform LZU-1 nanocrystals were synthesized by reacting NBPDA and TFB under microwave irradiation with PVP as the capping agent. In a typical synthesis, NBPDA and TFB were dissolved in 2 mL of ethanol with 10 mg/mL of PVP ($M_w = 360,000$) and 240 μL TFA, which was heated at 120 °C for 30 min to give a red suspension with protonated LZU-1 nanocrystals (Supporting Information, Section S9).¹⁴ This suspension rapidly turned yellow upon deprotonation by washing with an ethanol/triethylamine mixture (Supporting Information, Section S9). We believe the protonation of the imine COF renders the COF nanocrystals polar during crystal growth and allows PVP to bind and passivate their surface and regulate growth in alcoholic solution.

The size and morphology of the LZU-1 nanocrystals were characterized by SEM, which revealed their morphology and average size of 245 ± 25 nm (Figure 3a). The size of these nanocrystals can be tuned by the concentration of PVP, where 5 mg/mL of PVP gave 500 ± 52 nm COF particles and 40 mg/mL of PVP gave crystals of 112 ± 11 nm (Figure 3b and c). These particles were highly dispersible in ethanol and could remain colloidally stable for weeks (Figure 3d). Moreover, the morphology of COF nanocrystals can be tuned by solvent composition, where the addition of toluene into the ethanol growth solution yielded a hexagonal morphology. This hexagonal shape also supports the homogeneous nature of the crystal growth process and the high crystallinity of these nanocrystals (Figure 3e). The high crystallinity of these particles was also confirmed by HRTEM imaging, where the 2.2 nm hexagonal pore of the LZU-1 nanocrystal can be clearly observed as well as the 1D channels (Figure 3f and g), which is further supported by PXRD (Figure 3h).

The LZU-1 nanocrystals thus prepared display a high surface area of $729 \text{ m}^2/\text{g}$. This is more than 1.5 times that of the original report ($457 \text{ m}^2/\text{g}$) (Figure S21). Our synthetic method to produce COF nanocrystals is highly generalizable where two

different COFs, TFPB-PDA and Por-COF, were synthesized as nanocrystals (Figure S23). The microwave heating not only gives homogeneous rapid heating necessary for burst of nucleation but also allows for large-scale COF preparation. With 15 mL of solvent in one microwave vessel, a 100 mg scale of COF could be produced in 30 min, compared to sealing several Pyrex glass tubes and heating for days in the conventional methods. The utilization of the Boc-protected amine in a homogeneous synthetic route also broadens the range of conditions of COF synthesis, where solvents (i.e., alcohols) considered undesirable in conventional synthesis can now be used to give crystalline products. We believe these features will profoundly advance the application and fabrication of imine COFs. For example, the uniform and porous COF nanocrystals were used as well-defined processable building blocks in preparation of the COF-based mixed matrix membrane, where PVDF and LZU-1 nanocrystals were both dissolved in DMF and then casted into free-standing thin films with a surface area of $242 \text{ m}^2/\text{g}$ (Figure S24). With COFs nanocrystals below 200 nm, as their size was below the wavelength of visible light, the membrane became transparent. The homogeneous synthesis of imine COFs also allows for the fabrication of imine COFs into high-quality thin films. This can be demonstrated by synthesizing LZU-1 thin films on silicon substrates in hydrophobic aromatic solutions. As the protonated COF nanocrystals form homogeneously, the nucleation barrier would favor COF nucleation on the polar oxides, which would facilitate the selective growth of COF thin film on the substrates. The growth of imine COF thin film was realized by heating the substrate at 100 °C in the growth solution, where NBPDA and TFB were dissolved in a solvent mixture of toluene, dioxane, and TFA. A uniform film was formed after 2 h on the silicon substrate and the wall of the vial. The thin-film morphology of the COF can be clearly observed by SEM at the edge of the substrate where the film was partially detached (Figure 4a). Higher magnification SEM on the film revealed that it was composed of the small crystallites with potentially similar orientation (Figure 4b). The thickness of the film was measured by cross-section SEM to be 190 nm. It can be tuned empirically by changing the reaction time and concentration of the growth solution (Figure 4c and Supporting Information, Section S10). The crystallinity and orientation of the film were

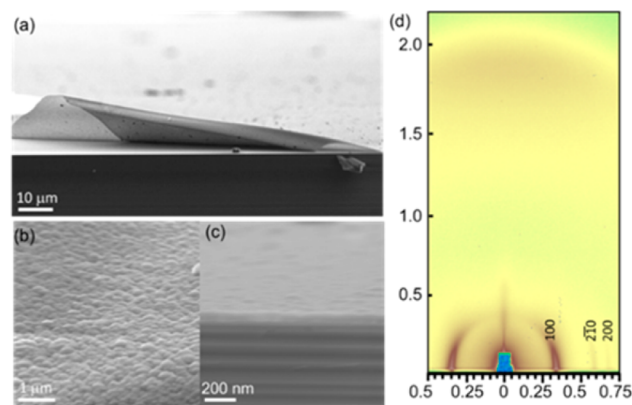


Figure 4. LZU-1 COF thin film prepared using NBPDA as starting material. The thin film was highly uniform (a) and composed of small crystallites with similar orientation (b). The thickness of the film was determined to be 190 nm by cross-sectional SEM (c) and its crystallinity and orientation confirmed by GIWAXS pattern (d).

characterized by GIWAXS measurements. Here, the 2D plane of the LZU-1 COF being flat on the substrate was revealed as having its [001] direction perpendicular to the substrate (Figure 4d). The high-quality COF film enabled us to measure its optical property by ellipsometry for the first time. Surprisingly, the highly porous material had a high refractive index of 1.83 at 632.8 nm wavelength. This is higher than most polymer materials and indicates the high level of in-plane conjugation in the COF. The high film quality and well-defined optical property give rise to interesting chemical-sensitive optical properties that indicate the porosity of these thin films (Supporting Information, Section S10). The homogeneous COF growth enabled by protected amine building blocks gives unprecedented high-quality crystalline, oriented, porous COF thin films that would advance the impact of COF chemistry in optical and electronic applications.

■ ASSOCIATED CONTENT

■ Supporting Information

The Supporting Information is available free of charge on the ACS Publications website at DOI: 10.1021/jacs.7b07457.

Synthesis and characterization, structure model details, crystal structure refinement tables, PXRD patterns, gas adsorption isotherms (PDF)

Crystal structure of COF-112 (CIF)

Crystal structure of $\text{Co}(\text{NH}_2\text{-DIP})_2(\text{BF}_4)_2$ complex (CIF)

■ AUTHOR INFORMATION

Corresponding Author

*yaghi@berkeley.edu

ORCID

Yingbo Zhao: 0000-0002-6289-7015

Lei Guo: 0000-0003-0013-3236

Felipe Gándara: 0000-0002-1671-6260

Eugene A. Kapustin: 0000-0003-4095-9729

Omar M. Yaghi: 0000-0002-5611-3325

Author Contributions

[#]These authors contributed equally.

Notes

The authors declare no competing financial interest.

■ ACKNOWLEDGMENTS

Material synthesis and characterization was supported by BASF SE (Ludwigshafen, Germany) and King Abdulaziz City for Science and Technology as part of a joint KACST–UC Berkeley collaboration (Center of Excellence for Nanomaterials and Clean Energy Applications). Work performed at the Advanced Light Source (beamline 7.3.3 and 11.3.1) and at the Molecular Foundry was supported by the Office of Science, Office of Basic Energy Sciences, of the U.S. Department of Energy under contract no. DE-AC02-05CH11231. We also acknowledge the Kavli energy nanoscience institute at UC Berkeley for support of research on nanostructuring of reticular materials. We thank Dr. S. Teat and Dr. L. McCormick for the synchrotron X-ray diffraction data acquisition support at the beamline 11.3.1 (Advanced Light Source, Lawrence Berkeley National Laboratory). We thank Dr. W. Bao for diffractive index measurement, Dr. N. Becknell, Ms. C. Xie for help with additional ALS study, Mr. P. Waller for help with organic synthesis, and Mr. C. S. Diercks for helpful discussion. Y.M. and

O.T. acknowledge support from ShanghaiTech Startup Funding and Shanghai Science and Technology Committee (17ZR1418600), Y.Z. acknowledges support from a SIP fellowship. L.G. acknowledges support from the Army Research Office for the Multidisciplinary University Research Initiatives award WG11NF-15-1-0047. F.G. acknowledges the Spanish Ministry of Economy and Competitiveness for funding through the Ramón y Cajal program. Z.L. acknowledges Prof. Sumio Iijima for supporting TEM measurements.

■ REFERENCES

- (1) Jiang, J.; Zhao, Y.; Yaghi, O. M. *J. Am. Chem. Soc.* **2016**, *138*, 3255–3265.
- (2) (a) Umemura, A.; Diring, S.; Furukawa, S.; Uehara, H.; Tsuruoka, T.; Kitagawa, S. *J. Am. Chem. Soc.* **2011**, *133*, 15506–15513. (b) Kuo, C.-H.; Tang, Y.; Chou, L.-Y.; Sneed, B. T.; Brodsky, C. N.; Zhao, Z.; Tsung, C.-K. *J. Am. Chem. Soc.* **2012**, *134*, 14345–14348. (c) Lausund, K. B.; Nilsen, O. *Nat. Commun.* **2016**, *7*, 13578. (d) Zhao, Y.; Kornienko, N.; Liu, Z.; Zhu, C.; Asahina, S.; Kuo, T.-R.; Bao, W.; Xie, C.; Hexemer, A.; Terasaki, O.; Yang, P.; Yaghi, O. M. *J. Am. Chem. Soc.* **2015**, *137*, 2199–2202. (e) Cavka, J. H.; Jakobsen, S.; Olsbye, U.; Guillou, N.; Lamberti, C.; Bordiga, S.; Lillerud, K. P. *J. Am. Chem. Soc.* **2008**, *130*, 13850–13851.
- (3) (a) Furukawa, H.; Cordova, K. E.; O’Keeffe, M.; Yaghi, O. M. *Science* **2013**, *341*, 1230444. (b) Rungtaweeworanit, B.; Zhao, Y.; Choi, K. M.; Yaghi, O. M. *Nano Res.* **2016**, *9*, 47–58.
- (4) Smith, B. J.; Overholts, A. C.; Hwang, N.; Dichtel, W. R. *Chem. Commun.* **2016**, 52, 3690–3693.
- (5) Ding, S.-Y.; Gao, J.; Wang, Q.; Zhang, Y.; Song, W.-G.; Su, C.-Y.; Wang, W. *J. Am. Chem. Soc.* **2011**, *133*, 19816–19822.
- (6) Peng, Y.; Wong, W. K.; Hu, Z.; Cheng, Y.; Yuan, D.; Khan, S. A.; Zhao, D. *Chem. Mater.* **2016**, *28*, 5095–5101.
- (7) Liao, H.; Wang, H.; Ding, H.; Meng, X.; Xu, H.; Wang, B.; Ai, X.; Wang, C. *J. Mater. Chem. A* **2016**, *4*, 7416–7421.
- (8) (a) Uribe-Romo, F. J.; Hunt, J. R.; Furukawa, H.; Klöck, C.; O’Keeffe, M.; Yaghi, O. M. *J. Am. Chem. Soc.* **2009**, *131*, 4570–4571. (b) Xu, H.; Gao, J.; Jiang, D. *Nat. Chem.* **2015**, *7*, 905–912.
- (9) Liu, Y.; Ma, Y.; Zhao, Y.; Sun, X.; Gándara, F.; Furukawa, H.; Liu, Z.; Zhu, H.; Zhu, C.; Suenaga, K.; Oleynikov, P.; Alshammari, A. S.; Zhang, X.; Terasaki, O.; Yaghi, O. M. *Science* **2016**, *351*, 365–369.
- (10) (a) Blake, A. J.; Lavery, A. J.; Hyde, T. I.; Schroder, M. J. *J. Chem. Soc., Dalton Trans.* **1989**, 5, 965–970. (b) Vance, A. L.; Alcock, N. W.; Heppert, J. A.; Busch, D. H. *Inorg. Chem.* **1998**, *37*, 6912–6920. (c) Leigh, D. A.; Lusby, P. J.; Teat, S. J.; Wilson, A. J.; Wong, J. K. *Angew. Chem., Int. Ed.* **2001**, *40*, 1538–1543.
- (11) Spitzler, E. L.; Dichtel, W. R. *Nat. Chem.* **2010**, *2*, 672–677.
- (12) Zhang, Y.-B.; Su, J.; Furukawa, H.; Yun, Y.; Gándara, F.; Duong, A.; Zou, X.; Yaghi, O. M. *J. Am. Chem. Soc.* **2013**, *135*, 16336–16339.
- (13) (a) Li, Y.; Yang, C.-X.; Yan, X.-P. *Chem. Commun.* **2017**, 53, 2511–2514. (b) Kandambeth, S.; Mallick, A.; Lukose, B.; Mane, M. V.; Heine, T.; Banerjee, R. *J. Am. Chem. Soc.* **2012**, *134*, 19524–19527. (c) Chong, J. H.; Sauer, M.; Patrick, B. O.; MacLachlan, M. J. *Org. Lett.* **2003**, *5*, 3823–3826. (d) Wei, H.; Chai, S.; Hu, N.; Yang, Z.; Wei, L.; Wang, L. *Chem. Commun.* **2015**, 51, 12178–12181.
- (14) Popp, N.; Homburg, T.; Stock, N.; Senker, J. *J. Mater. Chem. A* **2015**, *3*, 18492–18504.